Immunosuppressor Binding to the Immunophilin FKBP59 Affects the Local Structural Dynamics of a Surface β-Strand: Time-Resolved Fluorescence Study†

Nathalie Rouviere,‡ Michel Vincent,§ Constantin T. Craescu,|| and Jacques Gallay*,§

LURE Laboratoire pour l'Utilisation du Rayonnement Electromagnétique, Université Paris-Sud, Bâtiment 209D, F-91405 Orsay cedex, France, Institut National de la Santé et de la Recherche Médicale U33, Hôpital de Bicêtre, 80 rue du Général Leclerc, F-94276 Le Kremlin-Bicêtre cedex, France, and Institut National de la Santé et de la Recherche Médicale U350, Institut Curie-Biologie, Bâtiment 112, Centre Universitaire, F-91405 Orsay cedex, France

Received September 11, 1996; Revised Manuscript Received April 3, 1997⊗

ABSTRACT: The interaction of the immunophilin domain of FKBP59 (FKBP59-I) with immunosuppressant drugs was investigated by steady-state and time-resolved fluorescence of tryptophan. One of the two Trp residues present in this protein (W89), conserved in almost all immunophilins, is buried in the hydrophobic core and participates in the immunosuppressant binding. By comparison with the highly homologous protein FKBP12, containing only the buried Trp, it has been concluded that its weak fluorescence is due to an atypical H-bond interaction involving the indole nitrogen and the Phe129 benzene ring. The second Trp residue (W59) in FKBP59-I is located on the external hydrophilic side of the 50−60 β-sheet [Craescu, C. T., Rouvière, N., Popescu, A., Cerpolini, E., Lebeau, M.-C., Baulieu, E.-E., & Mispelter, J. (1996) *Biochemistry 35*, 11045−11052] and is responsible for >95% of the fluorescence emission. The long lifetime of the major excited state, the large activation energy of thermal quenching, and the rotational correlation time distribution pattern suggest that its environment is not highly mobile. Binding of the immunosuppressant drugs FK506 and rapamycin leads to a ∼60% decrease of the fluorescence intensity without any change in the fluorescence emission maximum. Time-resolved measurements show that this "quenching" is due to a conformational change which depletes the long excited-state lifetime population to the profit of a more quenched minor excited state, which becomes prominent in the complexes. This is accompanied by a strong slowing of the indole ring dynamics in the case of FK506 and by a complete immobilization in the case of rapamycin, as shown by two-dimensional (τ, θ) maximum entropy analysis of the polarized fluorescence decays. Binding of the immunosuppressant drugs therefore modifies the structure and the dynamics of the external side of the 50−60 β-sheet in FKBP59-I, which could be relevant for the formation of ternary complexes with other protein targets.

Immunosuppressant drugs such as cyclosporin or FK506 have been used, for at least 10 years, in medical transplantations to prevent graft rejection. More recently, receptors for these drugs were discovered and these proteins were called immunophilins. They bind either cyclosporin, like cyclophilins, or FK506, such as the FK506-binding proteins (FKBPs[1]). These ubiquitous proteins, of different sizes (10−80 kDa), seem to be involved in protein folding and/or to play a role in mitosis (Perrot-Applanat *et al.*, 1995; Lu *et al.*, 1996). Immunophilins exhibit peptidyl prolyl *cis*−*trans* isomerase (PPIase) activity, but their physiological substrate(s) remain(s) unknown. The immunosuppressive properties of the drugs are explained by the formation of an inactive ternary complex with calcineurin, a serine/threonine phosphatase (Liu *et al.*, 1991; Flanagan *et al.*, 1991).

FKBP59 was discovered in the hetero-oligomeric complexes containing nontransformed, non-DNA-binding, steroid receptors (Tai *et al.*, 1986, 1992). This protein is organized in three globular domains plus a fourth C-terminal domain, possessing specific and independent functional properties (Massol *et al.*, 1992; Le Bihan *et al.*, 1993; Radanyi *et al.*, 1994). In particular, the N-terminal domain (FKBP59-I), which is homologous to FKBP12, is responsible for the immunophilin character of the whole protein (Chambraud *et al.*, 1993). Although it shares with FKBP12 a similar PPIase activity, its affinity for FK506 is reduced by 2 orders of magnitude (Renoir *et al.*, 1994). Moreover, the binary complex (FK506−FKBP59) is not able to inhibit calcineurin phosphatase activity (Lebeau *et al.*, 1994). In an attempt to explain these functional differences, structural and dynamic studies were undertaken.

X-ray and NMR structures of an increasing number of immunophilins are presently available (Moore *et al.*, 1991; Michnick *et al.*, 1991; Van Duyne *et al.*, 1991a,b; 1993; Liang *et al.*, 1996a,b). Recently, we solved the solution structure of the N-terminal domain of FKBP59 using multinuclear and multidimensional NMR spectroscopy and restrained molecular dynamics (Rouvière-Fourmy *et al.*, 1995; Craescu *et al.*, 1996). The overall folding of the protein is characterized by a six-strand β-sheet and a hydrophobic α-helix. The three-dimensional structure is largely similar to that of FKBP12, except for the presence

† Supported by the Centre National de la Recherche Scientifique, the Institut Curie, the Institut National de la Santé et de la Recherche Médicale, and Rhône-Poulenc Rorer with a Bio-Avenir grant.

* Author to whom correspondence should be addressed (e-mail Gallay@lure.u-psud.fr).

‡ INSERM, Le Kremlin-Bicêtre.

§ LURE.

|| INSERM, Orsay.

⊗ Abstract published in *Advance ACS Abstracts,* May 15, 1997.

[1] Abbreviations: FKBP12, FK506-binding protein, 12 kDa; FKBP59, FK506-binding protein, 59 kDa; FKBP59-I, N-terminal domain (149 residues) of FKBP59; MEM, maximum entropy method; NATA, *N*-acetyltryptophanamide; PPIase, peptidyl-prolyl *cis*−*trans* isomerase; 3D, three-dimensional.

S0006-2960(96)02289-1 CCC: $14.00

of an additional β-strand at the N-terminal side. In particular, the residues involved in the drug binding site, which are all conserved, are superimposable. These data provide a basis for the understanding of the dynamic and functional properties of FKBP59-I. The presence of two tryptophan residues (W59 and W89) located in two different regions of the protein offers the opportunity to scrutinize in more detail the effects of ligand binding on the local structural dynamics, using steady-state and time-resolved fluorescence spectroscopy. We studied the immunophilin domain of FKBP59, both unliganded and liganded with immunosuppressants. Comparative studies were also performed with the homologous shorter immunophilin FKBP12, containing only the single tryptophan located in the binding site.

The major conclusion of our experiments is that drug binding elicits structural and dynamic changes affecting the solvent-exposed side of a β-strand, probed by the highly fluorescent W59, which is not in direct contact with the bound ligand. In contrast, W89, located in the drug binding site, is weakly fluorescent. It seems only slightly affected by ligand binding, in agreement with recent results on FKBP12 (Silva & Prendergast, 1996). Taken together, the present data suggest a possible mechanism by which ligand binding may control the interactions of the immunophilin with other target molecules, by modulating the side-chain dynamics of the hydrophilic molecular surface.

MATERIALS AND METHODS

Chemicals. Peptide substrates for PPIase assays were purchased from Bachem Biosciences (Horizon Drive, CA), and *N*-acetyltryptophanamide was from K&K (Plainview, NY). L-685,818 and L-683,590 were gifts from Pr. E.-E. Baulieu. FK506 was a kind gift from Fujisawa (Osaka, Japan), and rapamycin was a gift from Wyeth-Ayerst (Princeton, NJ). Other chemicals were at least of the reagent grade.

Protein Preparation. Construction and overexpression of the first domain of FKBP59 have been previously described (Chambraud *et al.*, 1993). Purification steps of FKBP59-I were performed according to the described procedures, and the purity was checked both by SDS−PAGE electrophoresis and by immunoblotting (Rouvière-Fourmy *et al.*, 1995). The standard buffer for enzymatic and fluorescence studies was Tris-HCl, 0.1 M, pH 7.8. FKBP12 was a generous gift of Vertex and of Dr. C. Radanyi.

Steady-State Enzymatic Studies. The PPIase rate was determined via isomerization of a peptidyl-containing peptide *N*-succinyl-Ala-Leu-Pro-Phe-*p*-nitroanilide (Harrison & Stein, 1990). Absorbance data points were performed at 400 nm on a Uvikon 930 spectrophotometer, and data points were fit to a first-order rate function using Graphit software on a PC computer. Measurements of k_{cat}/K_m for the PPIase activity were performed essentially according to described procedures (Park *et al.*, 1992; Rouvière-Fourmy *et al.*, 1995). The substrate specificity was checked for both full-length FKBP59 and the separated domains using peptides with a hydrophobic residue located just before the proline (Phe, Nor-Leu, Leu, Ile, Val, Ala). For each peptide substrate, the specific activity was found to be identical for domain I alone, for partial combinations such as I + II and I + II + III, or for total protein (I + II + III + IV). The highest values of k_{cat}/K_m were found for the Leu residue, as for FKBP12. Inhibition of PPIase activity by FK506, rapamycin, and two derivatives (L-685,818 and L-683,590) was performed using ethanol as the solvent for the stock solutions. Inhibition constants were determined using a competitive tight-binding equation, as described by Park *et al.* (1992).

Steady-State Fluorescence Measurements. Tryptophan fluorescence emission spectra were recorded between 300 and 420 nm (bandwidth = 4 nm) on a SLM 8000 spectrofluorometer equipped with Hamamatsu photon counting detectors (Model H3460-53) at an excitation wavelength of 295 nm (bandwidth = 2 nm) using 5 × 5 mm optical path cuvettes. Blanks were always subtracted in the same experimental conditions. The protein concentration for all fluorescence measurements was 1.2 μM in Tris-HCl standard buffer. The fluorescence quantum yield of the protein was calculated from the fluorescence intensities of three standards: indole in aerated ethanol (quantum yield = 0.27; De Lauder & Wahl, 1971), *p*-terphenyl in cyclohexane (quantum yield = 0.93; Berlman, 1971), and NATA in water (quantum yield = 0.103; our own measurements). To remove polarization artifact, the fluorescence emission spectra were reconstructed from the four polarized spectra according to

$$I(\lambda) = I_{vv}(\lambda) + 2G(\lambda)I_{vh}$$

where $G(\lambda)$ is a correction factor defined as

$$G(\lambda) = I_{hv}(\lambda)/I_{hh}(\lambda)$$

and $I_{vv}(\lambda)$, $I_{vh}(\lambda)$, $I_{hv}(\lambda)$, and $I_{hh}(\lambda)$ are the polarized fluorescence intensities at the emission wavelength λ after corresponding blank subtraction. The first and second subscripts refer to the orientation of the excitation and emission polarizers, respectively.

Evaluation of the dissociation constant of immunosuppressive ligands was performed with concentrations of both FK506 and rapamycin in the range of 0.01−3 μM.

Steady-state quenching measurements by acrylamide were realized with unliganded immunophilin domain, with FK506 complex and with NATA as reference. The intensities were corrected for the dilution and the inner filter effect due to the added acrylamide, taking into account the OD at the excitation wavelength.

Steady-state anisotropy excitation spectra were obtained with the same SLM 8000 spectrofluorometer operating in the T-format mode. Excitation wavelength was selected by a single holographic grating monochromator (bandwidth = 1 nm), and the fluorescence light was selected through a combination of one interference filter Schott 360 (10 nm bandwidth) and one cutoff filter (Schott WG 335). The protein samples were dissolved in glycerol/buffer mixture (80% glycerol w/w) at a concentration of 3 μM, and the temperature was maintained at −46 °C with a Hüber HS 60 cryothermostat. The steady-state anisotropy was calculated as a function of the excitation wavelength after appropriate blank subtraction:

$$A(\lambda) = \frac{I_{vv}(\lambda) - G(\lambda)I_{vh}(\lambda)}{I_{vv}(\lambda) + 2G(\lambda)I_{vh}(\lambda)}$$

Time-Resolved Fluorescence Measurements. Fluorescence intensity and anisotropy decays were obtained by the time-correlated single photon counting technique from the $I_{vv}(t)$

and $I_{vh}(t)$ components recorded on the experimental setup installed on the SB1 window of the synchrotron radiation machine Super-ACO (Anneau de Collision d'Orsay), which has been already described (Vincent *et al.*, 1995). The excitation wavelength was selected by a double monochromator (Jobin Yvon UV-DH10, bandwidth = 4 nm). A MCP-PMT Hamamatsu (Model R3809U-52) was used. Time resolution was ~20 ps, and the data were stored in 2048 channels. Automatic sampling cycles including 30 s accumulation time for the instrument response function and 90 s acquisition time for each polarized component were carried out until a total number of $(2-4) \times 10^6$ counts was reached in the fluorescence intensity decay.

Data Analysis. Analyses of fluorescence intensity and anisotropy decays as sums of exponentials were performed according to the maximum entropy method (Livesey *et al.*, 1986; Livesey & Brochon, 1987; Brochon, 1994). Details of the principles and application of the method to fluorescence decays have been previously published (Vincent *et al.*, 1988, 1992; Mérola *et al.*, 1989; Gentin *et al.*, 1990; Kuipers *et al.*, 1991; Gallay *et al.*, 1993; Bouhss *et al.*, 1996). They will be summarized in the following.

In the more general case where a chromophore is emitting with a lifetime τ and rotates with a rotational correlation time θ, the expression of each polarized fluorescence intensity decay is

$$I_{vv}(t) = \int_0^\infty \int_0^\infty \int_{-0.2}^{0.4} \gamma(\tau, \theta, A)\, e^{-t/\tau}(1 + 2A\, e^{-t/\theta})\, d\tau\, d\theta\, dA \quad (1)$$

and

$$I_{vh}(t) = \int_0^\infty \int_0^\infty \int_{-0.2}^{0.4} \gamma(\tau, \theta, A)\, e^{-t/\tau}(1 - A\, e^{-t/\theta})\, d\tau\, d\theta\, dA \quad (2)$$

where $\gamma(\tau, \theta, A)$ is the chromophore population with lifetime τ, rotational correlation time θ, and intrinsic anisotropy A. If a single intrinsic anisotropy value A is expected, as for the case of only one chromophore, the above expressions can be simplified as

$$I_{vv}(t) = \int_0^\infty \int_0^\infty \Gamma(\tau, \theta)\, e^{-t/\tau}(1 + 2A\, e^{-t/\theta})\, d\tau\, d\theta \quad (3)$$

$$I_{vh}(t) = \int_0^\infty \int_0^\infty \Gamma(\tau, \theta)\, e^{-t/\tau}(1 - A\, e^{-t/\theta})\, d\tau\, d\theta \quad (4)$$

The recovered distribution $\Gamma(\tau, \theta)$, which maximizes the entropy function S, is chosen (Jaynes, 1983; Livesey & Skilling, 1985):

$$S = \int_0^\infty \int_0^\infty \left[\Gamma(\tau, \theta) - m(\tau, \theta) - \Gamma(\tau, \theta) \log \frac{\Gamma(\tau,\theta)}{m(\tau, \theta)}\right] d\tau\, d\theta \quad (5)$$

In this expression, $m(\tau, \theta)$ is the starting model chosen as a flat surface over the explored (τ, θ) domain, since no *a priori* knowledge about the final distribution is available (Livesey & Brochon, 1987; Brochon, 1994). The analysis is bound by the constraint

$$\sum_{k=1}^{M} \frac{(I_k^{calcd} - I_k^{obs})^2}{\sigma_k^2} \leq M \quad (6)$$

where I_k^{calcd} and I_k^{obs} are the kth calculated and observed intensities. σ_k^2 is the variance of the kth point (Wahl, 1979). M is the number of (independent) observations of the fluorescence intensity at times t (Livesey & Brochon, 1987).

In the analysis of the data, the A value should therefore be introduced as a fixed parameter. This value can be determined, for instance, by steady-state anisotropy measurements in the absence of rotational motion as in vitrified solvents at low temperatures such as glycerol or propylene glycol at −50 °C. For FKBP59-I we have used the average value obtained by the one-dimensional analysis of the anisotropy decays described below and that measured in glycerol 80% w/w at −46 °C ($A = 0.193 \pm 0.013$ at 295 nm as excitation wavelength). For FKBP12, we have used the published value of 0.166 at the same excitation wavelength (Silva & Prendergast, 1996).

In principle, such an analysis allows description of lifetime heterogeneity and detection of the possible association between one particular excited-state lifetime of the fluorophore and its rotational correlation time. There is nevertheless an inherent limit to this method since, as shown from eqs 3 and 4, the parallel and the perpendicular components of the polarized decay involve in their expressions a harmonic mean κ_i between τ_i and θ_i

$$1/\kappa_i = 1/\tau_i + 1/\theta_i \quad (7)$$

where τ_i and θ_i can be exchanged without any modification in the κ_i value, leading to construction of iso-kappa curves (Gentin *et al.*, 1990). This degeneracy is especially troublesome when short lifetimes are coupled to long correlation times and conversely as shown by simulations (Brochon, 1994). A means to overcome this degeneracy is to use acrylamide as a quencher to decrease the lifetime values without altering the rotational correlation time ones.

Calculations were performed on a DEC alpha computer Vax 7620. The program including the MEMSYS 5 subroutines was writen in double-precision FORTRAN 77. CPU time of ~10 h was required to achieve the global analysis of $I_{vv}(t)$ and $I_{vh}(t)$ with 40 values, respectively, for τ and θ.

Excited-state Lifetime Distribution. In practice, an analysis of the fluorescence intensity decay is first performed. The intensity can be classically reconstructed from the polarized fluorescence decays by adding the parallel and twice the perpendicular components:

$$T(t) = I_{vv}(t) + 2\beta_{corr} I_{vh}(t) = \int_0^\infty \alpha(\tau) \exp(-t/\tau)\, d\tau \quad (8)$$

β_{corr} is the correction factor (Wahl, 1979) taking into account the difference of transmission of the polarized light components by the optics, and $\alpha(\tau)$ is the lifetime distribution.

The recovered distribution $\alpha(\tau)$ that maximizes the entropy function S is chosen:

$$S = \int_0^\infty \left[\alpha(\tau) - m(\tau) - \alpha(\tau) \log \frac{\alpha(\tau)}{m(\tau)}\right] d\tau \quad (9)$$

In this expression, $m(\tau)$ is the starting model and $\alpha(\tau)$ is the target distribution. In every analysis, a flat map over the

explored (τ) domain is chosen for $m(\tau)$, since no *a priori* knowledge about the final distribution is available.

The center τ_j of a single class j of lifetimes over the $\alpha(\tau_i)$ distribution is defined as

$$\tau_j = \sum_i \alpha_i(\tau_i)\tau_i / \sum_i \alpha_i(\tau_i) \quad (10)$$

the summation being performed on the significant values of the $\alpha(\tau_i)$ for the j class. C_j is the normalized contribution of the lifetime class j.

One-Dimensional Rotational Correlation Time Distribution. If all of the emitting species are assumed to display the same intrinsic anisotropy and rotational dynamics, eqs 1 and 2 can be rewritten as

$$I_{vv}(t) = \int_0^\infty \alpha(\tau)\, e^{-t/\tau}\, d\tau\, [1 + 2\int_0^\infty \beta(\theta)\, e^{-t/\theta}\, d\theta] \quad (11)$$

and

$$I_{vh}(t) = \int_0^\infty \alpha(\tau)\, e^{-t/\tau}\, d\tau\, [1 - \int_0^\infty \beta(\theta)\, e^{-t/\theta}\, d\theta] \quad (12)$$

with

$$A = \int_0^\infty \beta(\theta)\, d\theta \quad (13)$$

where $\beta(\theta)$ is the rotational correlation time distribution and the other symbols have the same significance as in eq 1. The $\alpha(\tau)$ profile is given from a first analysis of $T(t)$ by MEM and is held constant in a subsequent and global analysis of $I_{vv}(t)$ and $I_{vh}(t)$ which provides the distribution $\beta(\theta)$ of correlation times (Vincent & Gallay, 1991; Blandin *et al.*, 1994; Brochon, 1994). One hundred rotational correlation time values, equally spaced in logarithmic scale and ranging from 0.01 to 50 ns, were used for the analysis of $\beta(\theta)$.

The barycenters of the correlation time distribution are calculated as

$$\theta_j = \sum_i \beta_i(\theta_i)\theta_i / \sum_i \beta_i(\theta_i) \quad (14)$$

β_i is the contribution of the rotational correlation time i to the class j.

Wobbling Angle Calculation. Following Karplus formalism (Ichiye & Karplus, 1983), if the fast rotational motion decays exponentially with a relaxation time θ and reaches a plateau value P_∞, we have

$$A(t) = A\,[(1 - P_\infty)\exp(-t/\theta) + P_\infty]\exp(-t/\theta_m) \quad (15)$$

where θ_m is the overall rotational correlation time of the protein and A the intrinsic anisotropy.

If the fast rotational motion corresponds to a correlation function that separates into two time scales (θ_1 and θ_2), the expression of the anisotropy can be written as

$$A(t) = A\,\{[(1 - P_{\infty,1})\exp(-t/\theta_1) + P_{\infty,1}]\,[(1 - P_{\infty,2})\exp(-t/\theta_2) + P_{\infty,2}]\}\exp(-t/\theta_m) \quad (16)$$

with $\theta_1 \ll \theta_2 \ll \theta_m$. $P_{\infty,i}$ are the plateau values of the correlation function describing these internal motions.

The above expression of the anisotropy decay can be approximated by

$$A(t) = \beta_1 \exp(-t/\theta_1) + \beta_2 \exp(-t/\theta_2) + \beta_3 \exp(-t/\theta_m) \quad (17)$$

where $\beta_1 = (1 - P_{\infty,1})A$, $\beta_2 = P_{\infty,1}(1 - P_{\infty,2})A$, and $\beta_3 = P_{\infty,1}P_{\infty,2}A$.

In principle, if the time resolution of the experiment is such that it allows the description of all the rotational motions, the time-zero value of the anisotropy ($A_{t=0} = \Sigma\beta_j$) must be equal to the A value measured in the total absence of molecular motion. If short rotations (<50 ps) cannot be resolved, the extrapolated $A_{t=0}$ value can be smaller than the A value. The order parameter (S_1) associated with the subnanosecond motion of the indole ring can be indirectly calculated by using the $A_{t=0}$ and A values, as described by Levy and Szabo (1982).

The cone semiangle (ω_{max}) of the *subnanosecond rotation* of the fluorophore transition dipole (Kinosita *et al.*, 1977; Lipari & Szabo, 1980) and the associated orientational order parameter (S_1) can be calculated from

$$(\beta_2 + \beta_3)/A = P_{\infty,1} = {S_1}^2 = [1/2 \cos\omega_{max}\,(1 + \cos\omega_{max})]^2 \quad (18)$$

The application of such a model to the Trp motion inside a protein is only for the sake of comparison, since the geometry of the motion remains unknown. Moreover, strictly speaking, this model is limited to single-lifetime decays. If multiexponential decays are expected, the two-dimensional analysis should be tried to detect the possible associations between lifetime and rotational dynamics.

RESULTS AND DISCUSSION

Comparison of the Steady-State and Time-Resolved Fluorescence of Unbound FKBP59-I and FKBP12: Assignment of the Respective Signals of W59 and W89 and Characterization of Their Environment. The fluorescence emission spectrum of the uncomplexed FKBP59-I at 20 °C, excited in the Trp absorption spectral region, displays a maximum at 343 nm and is characterized by a relatively high quantum yield (Table 1). The fluorescence emission originates, in principle, from the excitation of the two Trp residues situated at positions 59 and 89 in the protein sequence. These residues are located in two distinct regions of the protein, according to the 3D structure of FKBP59-I determined in our laboratory (Craescu *et al.*, 1996): W59 is present at the external face of the 50−60 β-strand, and W89 is buried at the bottom of the drug binding site. This last residue is well-conserved in almost all immunophilins and is critical for the binding potency. The respective locations of these residues in the protein structure are shown in Figure 1. Since the FKBP59-I is highly homologous to the single-Trp-containing FKBP12 (W89 in the sequence numbering of FKBP59), a comparison of the fluorescence emission of both proteins is worthwhile, in order to estimate the relative proportions of the fluorescence signal that can be ascribed to each emittor in FKBP59-I.

Significant differences in the position of the fluorescence emission spectra of the two proteins are observed: the fluorescence emission spectrum of the single-Trp-containing protein FKBP12 is significantly blue-shifted with respect to that of FKBP59-I, in agreement with the hydrophobic location of W89 (Table 1). The fluorescence quantum yield

Table 1: Steady-State and Fluorescence Emission Decay Parameters of Free FKBP59-I (1.3 μM), Free FKBP12 (21 μM), FKBP59-I Complexed to FK506 and to Rapamycin (8 μM), and FKBP-12 Complexed to FK506 (8 μM)[a]

sample	quantum yield	λ_{max} (nm)	τ_1 (ns) (c_1)	τ_2 (ns) (c_2)	τ_3 (ns) (c_3)	τ_4 (ns) (c_4)	$\langle\tau\rangle$ (ns)	τ_0 (ns)
FKBP59-I	0.19	343.5	0.31 ± 0.10 (0.20 ± 0.08)	2.48 ± 0.45 (0.08 ± 0.01)	6.16 ± 0.47 (0.72 ± 0.07)		4.76	25.1
FKBP59-I/FK506	0.07	343.5	0.25 ± 0.11 (0.13 ± 0.05)	1.23 ± 0.03 (0.16 ± 0.03)	2.44 ± 0.03 (0.68 ± 0.04)	7.28 ± 0.79 (0.03 ± 0.003)	2.10	30.0
FKBP59-I/rapamycin	0.08	343.5	0.35 ± 0.07 (0.14 ± 0.09)	1.44 ± 0.14 (0.11 ± 0.08)	3.33 ± 0.09 (0.75 ± 0.04)		2.70	33.7
FKBP12	0.025	338.5	0.21 (0.80)	0.73 (0.11)	2.43 (0.07)	5.26 (0.02)	0.52	20.8
FKBP12/FK506	nd[b]	nd	0.14 (0.83)	1.21 (0.11)	3.78 (0.06)		0.48	nd

[a] Both barycenters (τ_j) of each lifetime peak and their normalized contributions (c_j) are listed. The average lifetime values were calculated according to $\langle\tau\rangle = \Sigma c_j\tau_j/\Sigma c_j$. The standard deviations of the centers of the peaks and of the normalized contribution for at least three measurements are reported for FKBP59-I. As a control and for the sake of comparison with published data (Silva & Prendergast, 1996), only one measurement was performed for FKBP12 and its complex with FK506, but the standard deviations should be similar. [b] Not determined.

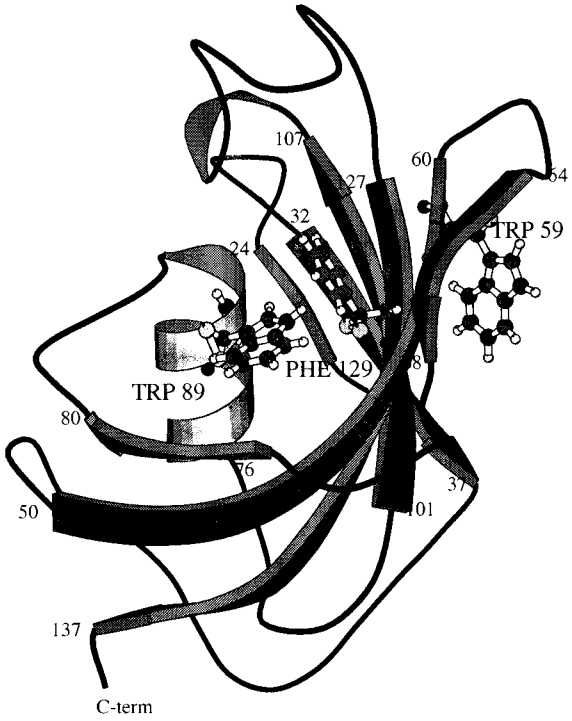

FIGURE 1: Location of the two tryptophans in FKBP59-I, relative to the protein backbone three-dimensional structure.

of FKBP12 is about 1 order magnitude lower than that of FKBP59-I (Table 1), in agreement with recently published results (Silva & Prendergast, 1996). These two observations suggest that the major fluorescent group in FKBP59-I is W59 (at the surface of the molecule) and not W89 (in the drug binding site).

The fluorescence decay of the single Trp in FKBP12 is dominated by a short lifetime of ~200 ps (Figure 2; Table 1), which corroborates recently published data (Silva & Prendergast, 1996). This lifetime corresponds to a fractional intensity of 31%. Three minor longer lifetimes are also observable. Although they are not present in high relative concentrations (as shown by the normalized amplitudes c_j), their contributions to the fluorescence signal are highly significant (15% for τ_2, 31% for τ_3, and 23% for τ_4). The current interpretation of this lifetime heterogeneity generally observed in proteins is that it corresponds to Trp conformers (Donzel *et al.*, 1974; Szabo & Rayner, 1980; Petrich *et al.*, 1983; Alcala *et al.*, 1987; Philips *et al.*, 1988; Chen *et al.*, 1991; Ross *et al.*, 1992; Willis *et al.*, 1994; Bouhss *et al.*, 1996). According to the tridimensional structure of the protein (Michnick *et al.*, 1991), a major χ_1, χ_2 conformer was ascribed by Silva and Prendergast (1996) as a g^-p^+ conformation. In this orientation, the indole ring points its NH group toward the center of the Phe129 phenyl ring (in the numeration of FKBP59). A similar conformation was also evidenced in the case of FKBP59-I (Craescu *et al.*, 1996). The aromatic rings are mainly perpendicular to each other (see Figure 1 for FKBP59-I). A strong shift of the Trp indole proton resonances due to shielding effect and a significant protection of the indole amine proton against exchange with deuterated water were observed (Rouvière-Fourmy *et al.*, 1995; Craescu *et al.*, 1996).

It appears therefore that the indole amino proton can form a peculiar hydrogen bond interaction with the proximate phenyl ring. The benzene ring may act as a H-bond acceptor because of the partial electronic charges on the carbon and hydrogen atoms (Levitt & Perutz, 1988). In such a configuration, mixing of the aromatic electron clouds may create an efficient nonradiative deactivation pathway. Moreover, this mixing can lead to modification of the energy gap and transition moments with regard to the native indole. The steady-state intrinsic excitation anisotropy spectrum of FKBP12 displays much lower values (Silva & Prendergast, 1996) than observed classically in proteins and in NATA (Valeur & Weber, 1977), in agreement with this proposal. The complex formed with the phenyl ring is analogous to that proposed for indole in benzene solution, where the existence of such H-bonding has been suggested (Van Duuren, 1961; Suwaiyan & Klein, 1989). The quenching efficiency is, however, stronger in the proteins than in benzene solution: the single excited-state lifetime value of indole in benzene is ~0.5 ns (Suwaiyan & Klein, 1989) as compared to ~0.2−0.3 ns, the shortest lifetime in the present proteins. This can be explained by the constraints in the binding site of proteins, which maintain the two aromatic residues at short distance (~3.5 Å), in a major perpendicular conformation (more efficient for fluorescence quenching) rather than in a less efficient parallel conformation.

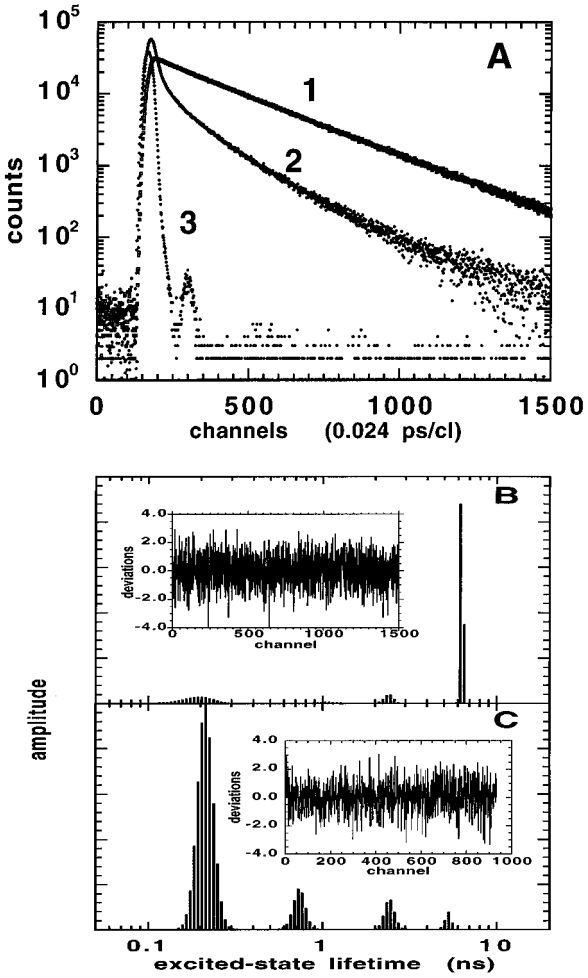

FIGURE 2: (A) Time course of the tryptophan fluorescence emission decay of (1) FKBP59-I and (2) FKBP12 and (3) instrumental response function. (B) Excited-state lifetime spectrum recovered by MEM analysis of the FKBP59-I data with 150 exponentials equally separated in log τ scale. (Insert) Weighted residuals. Excitation wavelength = 295 nm; emission wavelength = 345 nm; temperature = 20 °C; protein concentration = 1.2 μM. (C) Excited-state lifetime spectrum recovered by MEM analysis of the FKBP12 data with 150 exponentials equally separated in log τ scale. (Insert) Weighted residuals. Excitation wavelength = 295 nm; emission wavelength = 340 nm; temperature = 20 °C; protein concentration = 21 μM.

Nevertheless, the minor long-lived excited states that are also observed indicate the existence of a conformational heterogeneity leading to changes in the inter-ring distance and/or orientation, which have been shown to be of prime importance for the free energy of interaction between the NH group and the aromatic ring (Levitt & Perutz, 1988). Molecular dynamic calculations performed on FKBP12 have accredited the existence of one minor conformer tp^+ that does not display such an interaction since the indole nitrogen is oriented in the opposite direction of the major conformation (Silva & Prendergast, 1996). This is an extremely strong conformational alteration that can actually lead to a second discrete population with a longer lifetime value since the calculated interconverting rates between these two conformers are much longer than the average fluorescence decay time. The real situation seems, however, more complex since four lifetimes are obtained. More subtle conformational differences should therefore occur, implying perhaps these two major conformers.

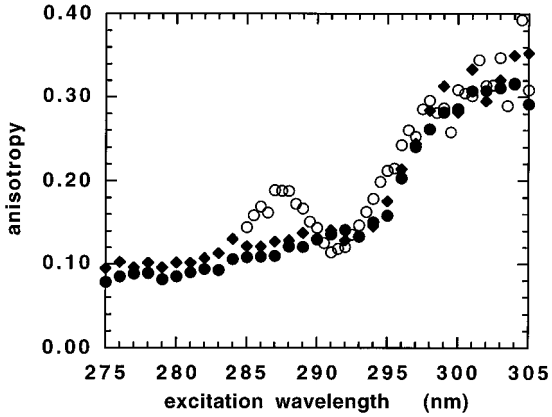

FIGURE 3: Steady-state excitation anisotropy spectra of unbound FKBP59-I (●), its complex with FK506 (◆), and NATA (○) in vitrified mixture of glycerol/buffer 80% (w/w) at −46 °C. Emission wavelength = 360 nm.

The Trp fluorescence emission decay of FKBP59-I is, by contrast with FKBP12, largely dominated by a long excited-state lifetime (Figure 2; Table 1) which represents 95% of the fluorescence intensity, in agreement with the high fluorescence quantum yield value. Two minor shorter lifetimes are also detected, particularly one of ~300 ps (Figure 2; Table 1). The similar values of the shortest lifetimes in both proteins suggest that it may originate from a common emittor, *i.e.* W89 in the ligand binding site. This lifetime becomes virtually undetectable at long emission wavelength (380 nm, data not shown), in keeping with observations from Eftink et al. (1987) on two-Trp-containing proteins, showing that short-lived Trp excited-state populations were often associated with blue emission (buried residues).

The direct association of the short-lived emittor in FKBP59-I with W89 is, however, not straightforward because relative amplitudes close to 0.5, or slightly smaller since other minor lifetimes are present in both proteins, should have been obtained. This is clearly not the case: the amplitude associated with the short lifetime is much smaller (0.20) and that of the long one is much higher (0.73) than the expected values (Table 1). A Trp-Trp resonant energy transfer mechanism may explain this fact. This was tested by measuring the steady-state anisotropy excitation spectrum at −46 °C in glycerol 80% w/w, a vitrified medium chosen to restrict rotational depolarization motions. In these conditions, the depolarization should only be due to the resonant energy transfer (Spencer & Weber, 1970). The results show that the steady-state anisotropy spectrum of FKBP59-I in the Trp specific absorption region (>290 nm) is close to that of NATA (Figure 3), which does not indicate a strong Trp-Trp resonant energy transfer. Therefore, at this stage, the hypothesis ascribing the short-lived excited state to the buried W89 residue needs to be more substantiated. This will be confirmed later on both by acrylamide quenching experiments and by two-dimensional analysis of the polarized fluorescence decays (Gentin *et al.*, 1990; Brochon, 1994).

The strong fluorescence and long excited-state lifetime of the surface-located tryptophan W59 indicates the absence of quenching interactions with either amino acid side chains or the protein main chain. Usually, dynamic quenching interactions with protein moieties (peptide bonds or protonated amino acid side chains) and also static quenching by disulfide bridges are occurring (Cowgill, 1962; Shinitzky & Goldman, 1967; Cowgill, 1967; Steiner & Kirby, 1969;

Table 2: Excited-State Lifetime Distribution Parameters of FKBP59-I Fluorescence Emission as a Function of Temperature[a]

temp (°C)	τ_1 (ns) (c_1)	τ_2 (ns) (c_2)	τ_3 (ns) (c_3)
5	0.45 (0.15)	2.41 (0.07)	6.96 (0.78)
10	0.46 (0.16)	2.87 (0.07)	6.77 (0.77)
15	0.42 (0.18)	2.63 (0.07)	6.51 (0.75)
20	0.44 (0.18)	2.82 (0.07)	6.20 (0.75)
30	0.39 (0.19)	1.91 (0.03)	5.52 (0.78)
40	0.35 (0.19)	1.99 (0.05)	4.82 (0.76)

[a] Excitation wavelength = 295 nm (bandwidth 4 nm); emission wavelength = 345 nm (bandwidth 10 nm).

Bushueva *et al.*, 1974, 1975; Ricci & Nesta, 1976; Petrich *et al.*, 1983; Shizuka *et al.*, 1988; Tilstra *et al.*, 1990; McMahon *et al.*, 1992; Vos & Engelborghs, 1994). No disulfide bridges are actually present in this protein, and the examination of its 3D structure (Craescu *et al.*, 1996) does not show evidence for presence of quencher groups in close proximity of W59 (the side chains of Lys55 and Arg103 are distant by ~8−10 Å from the indole nitrogen). The existence of one major narrow lifetime population is an indication of a well-defined major local conformation of the W59 indole ring without any large mobility. This is in agreement with recent NMR experiments that showed a large protection of this β-sheet region against amide proton exchange with the solvent (Craescu *et al.*, 1996).

Effect of Temperature on the Lifetime Distribution of FKBP59-I. Temperature-dependent time-resolved measurements show that a strong thermal quenching affects the long excited-state lifetime. The intermediate lifetime is slightly decreased, while the short one remains unaffected (Table 2). There is virtually no effect of temperature on the relative proportions of the three lifetimes from 5 to 40 °C (Table 2). Two radiationless deactivation pathways have been postulated to occur for indole (Kirby & Steiner, 1970; Walker *et al.*, 1969), one being temperature-insensitive ($k_{NR0} \sim 5-7 \times 10^7$ s^{-1}) (Gally & Edelman, 1962; Klein & Tatisheff, 1977; Suwaiyan & Klein, 1989) and the other being temperature-sensitive. The activation energy of the latter radiationless process was calculated from an Arrhenius representation using either the mean excited-state lifetime or the long lifetime to calculate the temperature-sensitive nonradiative rate constant at different temperatures. Linear fits were quite acceptable for both time constants (regression coefficients = 0.996 or 0.998) and gave activation energy values of 14.5 and 24 kcal mol^{-1}, respectively, for the average lifetime and the long one, significantly higher than the values measured in water solution (Klein & Tatisheff, 1977). This indicates that although W59 is located at the protein surface, more thermal energy is needed to provide efficient collisions of either solvent molecules or amino acid side chains. In other words, the microenvironment of this side chain is probably more rigid than generally expected for an exposed residue. This is further confirmed by anisotropy decay measurements for the rotation of the indole ring itself.

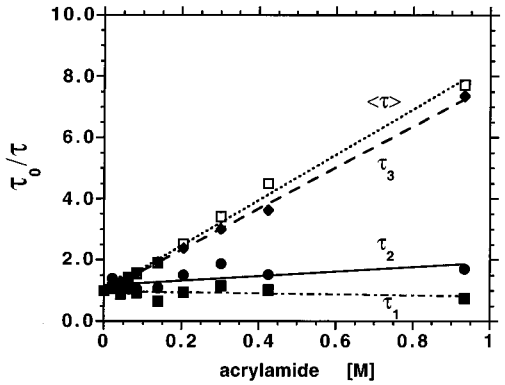

FIGURE 4: Stern−Volmer representation of the time-resolved data for FKBP59-I. Protein concentration = 10 μM.

Table 3: Static and Dynamic Acrylamide Quenching Constants for Free FKBP59-I and Complexed with FK506

sample	V (M^{-1})	K_{sv} (M^{-1})	$k_q \times 10^9$ (M^{-1} s^{-1})
FKBP59-I	2.1	7.4	1.6[a]
		6.7	1.1[b]
	2.2	9.3	1.95[c]
FKBP59-I/FK506	2.2	2.4	1.1[a]

[a] Values obtained with the mean lifetime. [b] Values obtained with the long lifetime. [c] Values obtained with steady-state measurements.

Acrylamide Quenching of FKBP59-I. An efficient acrylamide quenching is also observed both by steady-state and by time-resolved measurements. Steady-state Stern−Volmer plots for FKBP59-I and NATA are not linear but show upward curvatures (not shown). This feature has been ascribed to the coexistence of both static and dynamic quenching (Eftink & Ghiron, 1984). The quenching does not lead to any spectral displacement toward shorter emission wavelength, as could have been expected for a selective quenching of the more exposed W59. This is likely due to the much stronger emission of W59, which still dominates that of W89 even at the highest acrylamide concentration used (0.93 M).

The major effect of acrylamide on the protein time-resolved fluorescence is to reduce the value of the long lifetime. No evidence for fast transients was obtained in the fit of the fluorescence decay data by MEM for the whole set of acrylamide concentrations (Lakowicz *et al.*, 1987). The Stern−Volmer plots constructed either from the mean lifetime or from the long lifetime values were reasonably linear (correlation coefficients = 0.997 and 0.999, respectively) (Figure 4), in contrast to many other multi-tryptophan-containing proteins (Stryjewski & Wasylewski, 1986). The linearity of the time-resolved Stern−Volmer plot with the mean lifetime shows indeed that a single major quenching constant describes the quenching process for this two-Trp-containing protein. Similar k_q values (the bimolecular dynamic quenching constant) are obtained with either the mean lifetime or the long lifetime Stern−Volmer plots, although it is slightly higher for the former than for the latter one (Table 3). This difference may arise from the different susceptibility of the three lifetimes to acrylamide. More precisely, the intermediate lifetime is indeed less prone to acrylamide quenching than the long one as judged from the smaller bimolecular quenching constant value of 5×10^8 M^{-1} s^{-1} obtained from the linear fit of the Stern−Volmer plot for this lifetime as compared to that of the long lifetime

(Table 3). This lifetime may correspond to a minor conformer of either W59 or W89. The shortest lifetime remains insensitive to acrylamide: a mean value of 0.23 ± 0.04 ns is found for the whole titration. At 0.93 M acrylamide, its relative proportion rises to 43%, twice the value in the absence of quencher. This is in favor of the hypothesis ascribing this short lifetime to the buried W89.

The k_q value for FKBP59-I is much higher than that obtained for RNase T1 (Eftink, 1991), where the Trp residue is fully buried within the protein matrix. It is by contrast significantly smaller than the values for fully exposed Trp residues in small peptides such as ACTH, glucagon, or monomeric melittin (Eftink, 1991) and lower than for NATA in water (Eftink & Ghiron, 1976). This evidences the effective screening effect of the protein structure on the acrylamide diffusion despite its external location. The quenching constant is in fact of the same order of magnitude as that measured for Trp3 in porcine pancreatic phospholipase A_2, where the indole ring is parallel to the protein surface, when the heterogeneity of excited-state lifetimes is introduced into the model (Ludescher *et al.*, 1985; Eftink, 1991). A rough estimation of the fractional accessibility can be obtained according to the method of Johnson and Yguerabide (1985) by comparing the k_q value for the protein to that of NATA in water. We found a fractional accessibility of ~20% of the surface area of the fluorophore. This is corroborated by the Connolly surfaces of the two tryptophans, calculated using DSSP software (Kabsch & Sander, 1983) which gives values of 77 and 10 Å^2, respectively, for W59 and W89, compared to 384 Å^2 obtained for free tryptophan.

Binding of Immunosuppressants to FKBP59-I Affects the Dynamics of the Surface W59 Residue. FK506 or rapamycin binding induces a large decrease of the fluorescence intensity of FKBP59-I by 63% and 58% respectively, without any shift of the fluorescence emission spectra (Table 1), in contrast to FKBP12 for which the fluorescence quenching was accompanied by a red shift of the fluorescence emission spectrum upon binding of the immunosuppressive ligands (Silva & Prendergast, 1996). The decrease of fluorescence intensity follows a saturation curve for both ligands. The fluorescence intensity ratio (calculated from the integral of the fluorescence spectra) can be plotted as a percentage of saturation versus increasing inhibitor concentration. These data can be fit according to a hyperbolic nonlinear regression to obtain pseudo-dissociation constants. Their values are reported in Table 4.

The mechanism of the apparent fluorescence quenching by immunosuppressant binding to FKBP59-I was further studied by time-resolved measurements. The major effect of FK506 binding is a proportional decrease of the long-lifetime amplitude, which vanishes after titration completion, to the benefit of an intermediate lifetime component (~2.4 ns), which proportion saturates at ~70% (Figure 5). No progressive shift of the center of the long-lifetime population can be observed as it should be for a dynamic quenching process, such as acrylamide quenching (see above). The observed steady-state quenching following FK506 binding is fully accounted for by this excited-state population exchange. The ratio of the two major lifetimes respectively in the free and in the bound protein exhibits exactly the same value as the intensity ratio. Therefore, we are not faced with a dynamic quenching process resulting from a direct interaction of the ligand with the indole ring. Rather, we are dealing with an indirect effect of the ligand on the conformational equilibrium of that region of the protein surface, which changes the proportions of the W59 conformers, according to the conformer model commonly used to explain the fluorescence heterogeneity of Trp in solution (Donzel *et al.*, 1974; Szabo & Rayner, 1980). The lifetime distribution profile of the FKBP59-I/FK506 complex exhibits additional peaks which progressively appear upon saturation completion. Whether this is due to dynamical characteristics of the complex deserves further investigations.

Table 4: Pseudo-Binding and Inhibition Constants for FKBP-59 (Full-Length and Domains)

Pseudo-Binding Constants, K_D (in nM)		
protein	FK506	rapamycin
FKBP59-I[a]	202 ± 9	1160 ± 160
FKBP59-I[b]	417 ± 97	2860 ± 810

Inhibition Constants of PPIase Activity (in nM)				
protein	FK506	rapamycin	L-685	L-683
h FKBP12	0.42			
	0.6[c]	0.25[c]		
FKBP59-I	62 ± 29 (3)	45 ± 17 (2)	48 ± 17 (2)	47 ± 23 (2)
FKBP59-(I + II)[d]	51 ± 12 (2)	31 ± 18 (2)	39	55
FKBP59-(I + II + III)[d]	82	72		
FKBP59-(full length)[d]	41	43		

[a] Results obtained by using a nonlinear regression program of steady-state fluorescence data versus increasing ligand concentration. [b] Results obtained by using a nonlinear regression program of lifetime-resolved fluorescence data versus increasing ligand concentration. [c] Results taken from Park et al. (1992) under the same experimental conditions. [d] GST-fusion proteins were used. Experimental conditions: Assays were performed in 0.1 M Tris-HCl buffer, pH 7.8, at 15 °C. The peptide substrate was Suc-Ala-Leu-Pro-Phe-*p*-nitroanilide at a concentration of 60 mM, in the coupled chymotrypsin assay. The specific activity was calculated from $k_{obs} - k_{non-enz}$/[enzyme]; the concentration of enzyme was 40 nM. In parentheses: number of determinations.

The increase of the proportion of the intermediate lifetime and the decrease of the proportion of the long lifetime versus increasing FK506 drug concentration follow saturation curves (Figure 5, inset). Once again, a hyperbolic nonlinear regression fit gives values that agree with a lower affinity of the drug, and this is correlated with a lesser inhibition potential of the drug versus PPIase activity of FKBP59-I as compared to FKBP12 (Table 4).

Binding of rapamycin leads to essentially similar results: decrease of the relative proportion of the long lifetime, which cancels out at drug saturation, and parallel increase of the proportion of an intermediate lifetime, which saturates at 75% (see Figure 6). Slight differences can, however, be observed. In particular, the major excited-state lifetime in the final complex displays a significantly larger value in the rapamycin/FKBP59-I than in the FK506/FKBP59-I complex (Table 1). The lifetime distribution profile is simpler in the binary complex with rapamycin, pointing out differences in the structural dynamics of the two complexes, which remain to be precisely defined but that can be related to the different immobilization of the indole ring as described in the section concerning anisotropy measurements. Moreover, an examination of the pseudo-K_D values seems to indicate a different behavior of the two drugs with respect to the solvent-accessible tryptophan (see Table 4). This suggests that despite their large structural similarities, the two ligands do not bind to the protein exactly in the same orientation or position in the binding site. This is apparent in the crystal

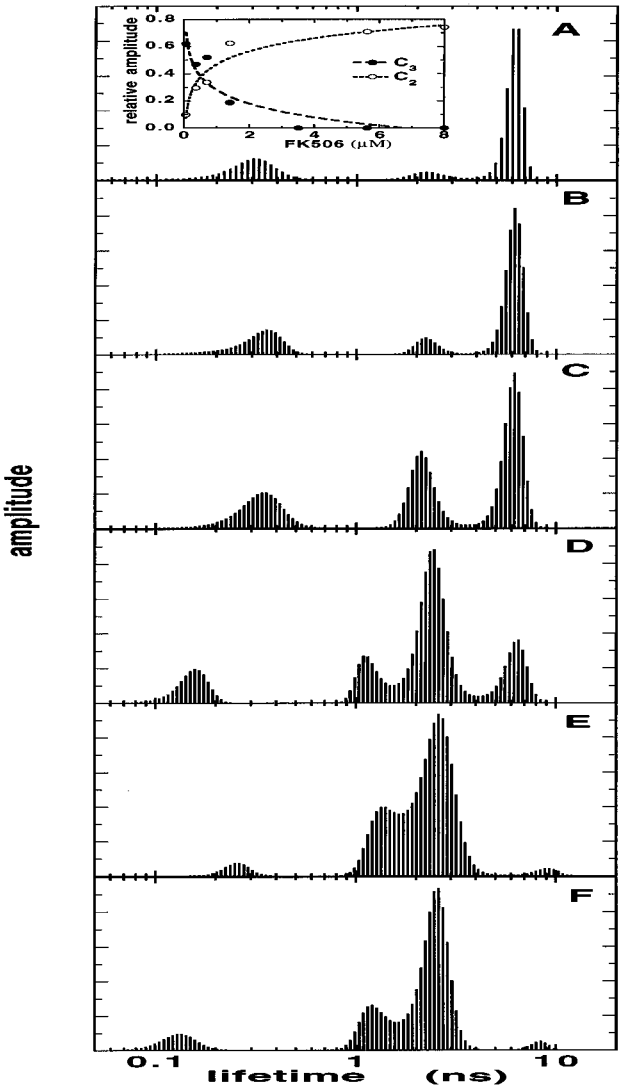

FIGURE 5: Excited-state lifetime profile of FKBP59-I as a function of FK506 concentration: (A) none; (B) 56 nM; (C) 362 nM; (D) 1.4 μM; (E) 5.62 μM; (F) 8 μM. Protein concentration, 1.2 μM. (Inset) Variation of the proportions of τ_2 and τ_3 as a function of FK506 concentration.

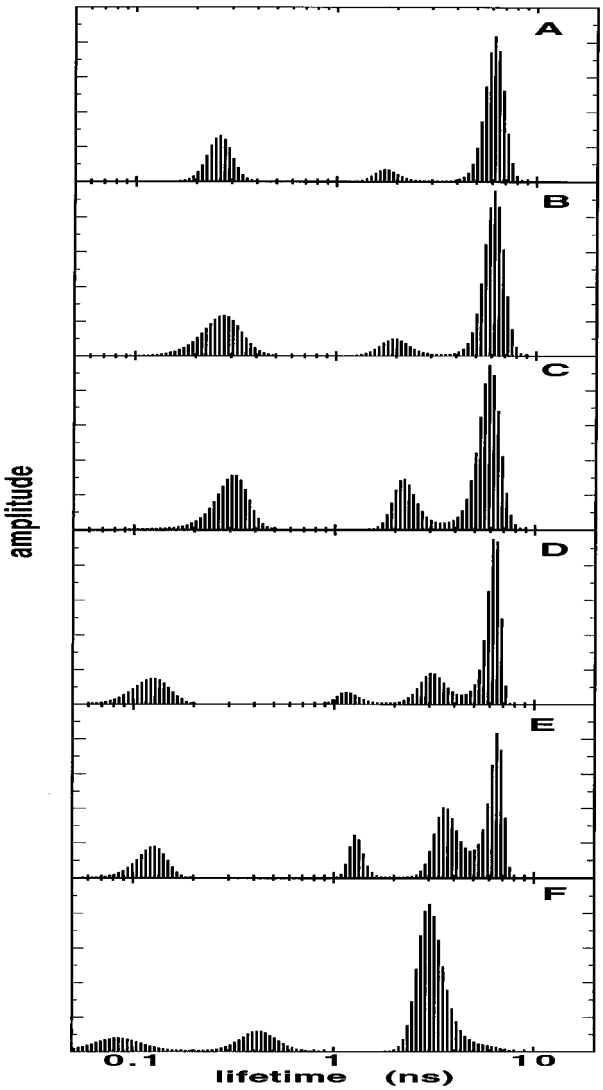

FIGURE 6: Excited-state lifetime profile of FKBP59-I as a function of rapamycin concentration: (A) none; (B) 56 nM; (C) 330 nM; (D) 800 nM; (E) 1.5 μM; (F) 8 μM. Protein concentration = 1.2 μM.

structures of both complexes with FKBP12 (Van Duyne *et al.*, 1991a,b). This can explain the subtle differences of environment of the surface Trp residue in both complexes, revealed by the lifetime distributions. It is noteworthy that neither the previously reported K_D values of both FK506 and rapamycin (Renoir *et al.*, 1994) nor K_I values (our present work) permitted such a discrimination for FKBP59-I. Since several drugs with subtle differences in solvent-exposed regions were also used (Rotonda *et al.*, 1993) and gave the same results as FK506 for inhibition (see Table 4), it would be interesting to further study their interaction with FKBP59-I by fluorescence. This is under current investigation.

Acrylamide quenching remains as efficient in the complex with FK506 as in the unbound protein. The Stern−Volmer plot of the time-resolved data for the FKBP59-I/FK506 complex is linear and gives a bimolecular quenching constant identical to that of the unbound protein (Table 3). This corroborates the idea that the W59 residue is not in direct contact with the ligand in FKBP59-I, in agreement with the known structure of the FKBP12/FK506 complex (Van Duyne *et al.*, 1991, 1993) and the recent data on FKBP59-I/FK506 complex (Rouvière *et al.*, unpublished results). This suggests also that the modification of the local conformation of the external face of the β-sheet probed by W59 is not strong enough to modify significantly the solvent accessibility of this residue (at least as probed by acrylamide). This is in agreement with the unchanged value of the fluorescence emission maximum with inhibitor binding.

Rotational Dynamics of the Trp Residues in FKBP12 and in FKBP59-I. The analysis of the FKBP12 polarized decays by the one-dimensional anisotropy model, which correlates all of the lifetimes with all of the flexibilities, fits reasonably well the data with a low chi-square value of ~1.05. One short subnanosecond correlation time of ~100 ps (β_1 = 0.022) and a long one of ~11 ns (β_2 = 0.123) are obtained (Figure 7A). We should remark, however, first, that the deviation function is not regularly distributed around zero value but exhibits some structure, second, that the correlation time distribution pattern shows some undefined increasing values at very short times, and, third, that the sum of the significant preexponential factors is well below the expected time-zero anisotropy value or intrinsic anisotropy value that has been recently measured ($A_{295\ nm}$ = 0.166) (Silva & Prendergast, 1996). This last point could, however, be due to the finite time resolution of our instrumentation.

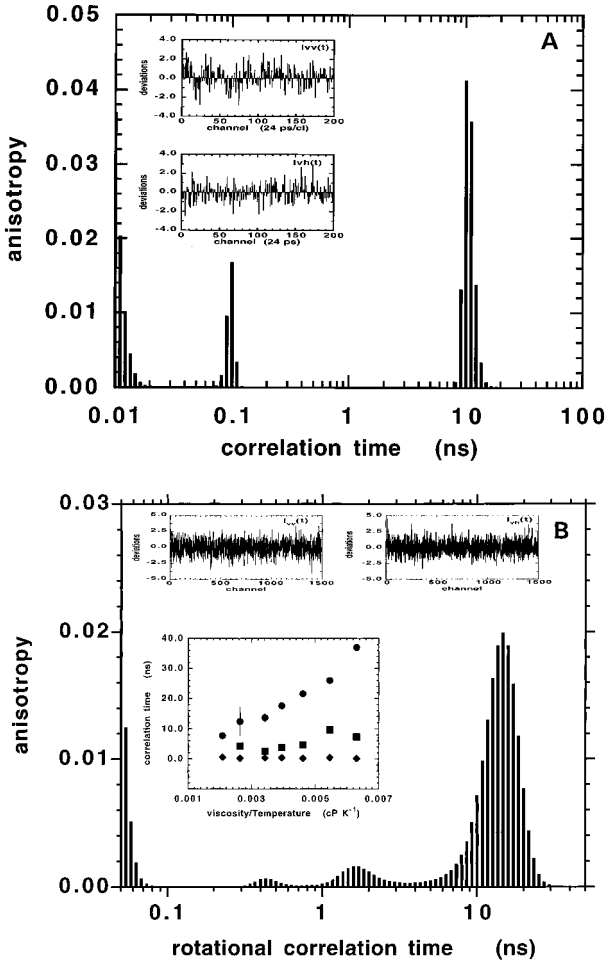

FIGURE 7: One-dimensional rotational correlation time distribution recovered by MEM. (A) FKBP12 [(insets) deviation functions of the weighted residuals for $I_{vv}(t)$ and $I_{vh}(t)$ (excitation wavelength = 295 nm; emission wavelength = 340 nm; temperature = 20 °C)]; (B) FKBP59-I [(upper insets) deviation functions of the weighted residuals for $I_{vv}(t)$ and $I_{vh}(t)$; (lower inset) Perrin plot of the thermal variation of the rotational correlation times: (●) rotational correlation time of the Brownian motion of the protein; (■) intermediate correlation time; (◆) fast rotation of the indole ring (excitation wavelength = 295 nm; emission wavelength = 345 nm; temperature = 20 °C)].

The impulse anisotropy response function that was calculated from the separate deconvolution of each polarized intensity decays does not show, however, a classical decay pattern but a characteristic shape presenting a fast decay during the first 500 ps followed by an intermediate increase in the nanosecond time range and finally by a further slow decrease (Figure 8A). The time-zero value of the anisotropy is lower than expected for 295 nm as excitation wavelength, but is in agreement with the steady-state anisotropy value measured in vitrified medium (Silva & Prendergast, 1996). This suggests in fact that the previous analysis is probably not adequate to use for this single-Trp-containing protein. This may be due to the fact that specific associations between lifetimes and rotational correlation times are prevailing, as was suggested from analysis of simulated data (Brochon, 1994). The intensity decay is dominated by a short lifetime that could be associated with a fast dynamics.

Therefore, a two-dimensional analysis was performed. For these calculations, the published value of the intrinsic anisotropy of 0.166 at the excitation wavelength of 295 nm was used (Silva & Prendergast, 1996). The result of the

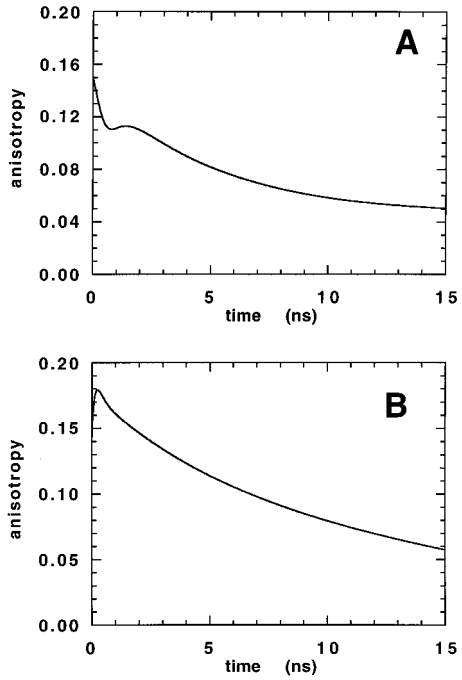

FIGURE 8: Impulse anisotropy decays of (A) FKBP12 and (B) FKBP59-I. Excitation wavelength = 295 nm; emission wavelength = 340 nm for curve 1 and 345 nm for curve 2; temperature = 20 °C.

analysis is represented as a two-dimensional (τ, θ) plot (Figure 9A). The diagram is largely dominated by a major peak associating the shortest lifetime and a ~1 ns correlation time. Minor peaks are also detectable; in particular, the 2.4 ns lifetime is only associated with a 6−7 ns correlation time, likely describing the Brownian motion of the protein, and not with any faster rotation.

These observations strengthen strongly the conformer hypothesis of W89, supported by molecular dynamic simulations (Silva & Prendergast, 1996). The local motion of the indole ring in the major conformer is nevertheless slow, 4−5 times slower than the excited-state lifetime with which it is associated. This conformer probably corresponds to the major g^-p^+ rotamer in the reported 3D structures, in strong interaction with the F129 phenyl ring. The second lifetime may correspond to the same rotamer since it moves with a similar flexibility, but with respective orientations of both aromatic rings slightly different from that in the major conformation. The minor long lifetimes in FKBP12 may correspond to the other minor conformer defined in the molecular dynamic calculation as a tp^+ conformation, which displays a completely different orientation with the indole NH group pointing to the opposite direction of the phenyl ring. It undergoes, therefore, poorly efficient quenching interactions with the phenyl ring.

The case of FKBP59-I is very different. As was amply discussed in preceding sections, the fluorescence emission of the protein is largely dominated by a long-lived excited state ascribed to the exposed Trp residue W59. Therefore, as a first approximation, we considered that it is almost a single excited-state decay which is obviously linked to all depolarizing rotational motions. This is confirmed by the low chi-square values obtained and the regular pattern of the deviation functions for $I_{vv}(t)$ and $I_{vh}(t)$ (Figure 7B, insert). The results of this analysis show three rotational correlation time populations in the subnanosecond and nanosecond time

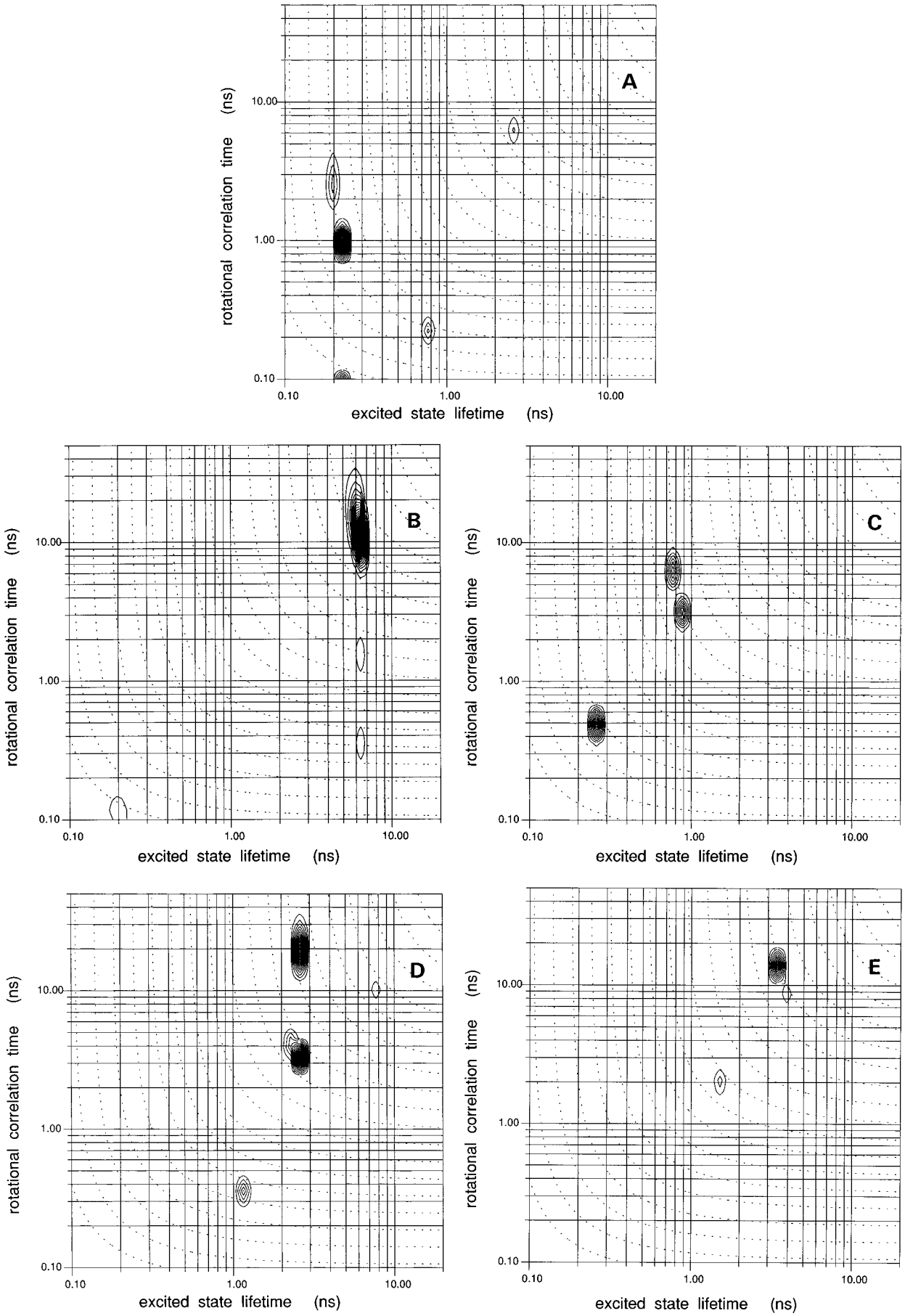

FIGURE 9: Two-dimensional (τ, θ) plots of FKBP12 (A), FKBP59-I (B), FKBP59-I quenched by 0.93 M acrylamide (C), FKBP59-I/FK506 complex (D), and FKBP59-I/rapamycin complex (E). Excitation wavelength = 295 nm; emission wavelength = 340 nm for curve A and 345 nm for curve B. *A* value for curve A = 0.166; for curves B−E = 0.193. Temperature = 20 °C. Dashed lines represents the iso-kappa curves defined under Materials and Methods.

Table 5: Fluorescence Anisotropy Decay Parameters of FKBP59-I Trp Emission Obtained by One-Dimensional Analysis[a]

temp (°C)	θ_3 (ns) (β_3)	θ_2 (ns) (β_2)	θ_1 (ns) (β_1)	ω_{max} (deg)
1	30.5 (0.154)	6.6 (0.035)	0.21 (0.027)	7
5	26.7 (0.120)	9.6 (0.059)	0.44 (0.010)	13
10	21.6 (0.151)	4.6 (0.033)	0.17 (0.007)	10
15	17.6 (0.161)	3.7 (0.020)	0.37 (0.013)	10
20	13.7 ± 1.3 (0.167 ± 0.001)	1.9 ± 0.7 (0.013 ± 0.004)	0.41 ± 0.09 (0.003 ± 0.001)	12 ± 3
20 FK506 complex	12.8 ± 0.6 (0.193 ± 0.011)			0
20 rapamycin complex	15.2 ± 0.1 (0.199 ± 0.003)			0 0
30	12.3 (0.138)	2.2 (0.021)	0.23 (0.013)	24
40	7.7 (0.159)		0.55 (0.006)	20

[a] Excitation wavelength = 295 nm (bandwidth 4 nm); emission wavelength = 345 nm (bandwidth 10 nm). The semiangle of the wobbling cone (ω_{max}) was calculated according to the method of Kinosita et al. (1977) with an average A value of 0.193 ± 0.013 in the absence of ligand. The standard deviations for four measurements at 20 °C are given.

scales (Figure 7B). These populations probably describe, respectively, the indole ring picosecond rotations, some nanosecond segmental flexibilities of the β-strand, and finally the Brownian rotation of the protein. This last motion, described by a rotational correlation time of 14 ns at 20 °C, dominates the fluorescence anisotropy decay. Its variation with temperature is approximately linear in η/T coordinates (Figure 7B, inset). The hydrated volume calculated from the slope of the plot is significantly larger than the one expected for a protein of this size. This may be due to the existence of flexible loops at both the N- and C-terminal ends of the protein.

At all temperatures below 40 °C, all of the rotational motions are detected since the average initial anisotropy value at zero time after the excitation pulse ($A_{t=0} = 0.193 \pm 0.013$), is very close to that of the intrinsic anisotropy measured at 295 nm as excitation wavelength in vitrified media (A = 0.189) (Figure 3). The intermediate rotational correlation time of small amplitude becomes shorter also with temperature increase, and at 40 °C, its value is similar to that of the fastest rotational correlation time (Figure 7B, inset). It may represent peptide segmental motions of the 50−60 β-strand supporting the Trp59 residue. Its contribution to the anisotropy shows a decreasing trend with increasing temperature (Table 5). This may indicate the existence of stabilizing hydrophobic interactions supported by nonpolar amino acid side chains in the inner side of the β-strand such as V52 and 54. Y56 and G58, close to W59, are implicated in hydrophobic contacts with the immunosuppressants and could take part in the effect.

At 40 °C, only two motions are detectable and, in contrast with other temperatures, the initial anisotropy value is lower than the intrinsic anisotropy value. This shows that at this temperature fast unmeasurable motions with our instrumentation (<50−100 ps) are occurring. Nevertheless, at all temperatures the major depolarization motion is the Brownian rotational diffusion; the subnanosecond internal dynamics plays only a minor contribution. The amplitude of the indole subnanosecond motion is small, as can be seen from the weak value of the wobbling-in-cone semiangle of the subnanosecond rotational motion of the indole ring. It increases at temperatures >30 °C (Table 5). The subnanosecond rotational motions of W59 appear therefore to be severely limited by the local protein structure, but it is thermally sensitive. This may explain the large activation energy of the thermal quenching previously observed.

These analyses were performed and interpreted in first approximation as if a single emittor (the Trp residue at the protein surface) were present in the protein. The short lifetime which is likely associated with the emission of the second Trp residue (W89) is, however, responsible for a few percent of the fluorescence emission, especially in the subnanosecond time domain. It may therefore play its own part in this short time region. The impulse anisotropy decay curve, calculated from the deconvolved polarized fluorescence decays, shows a regular decreasing pattern except at very short time, where an increase of the anisotropy with time can be observed (Figure 8B), which may be the signature of the short-lived emittor. The two-dimensional analysis was therefore performed to provide a specific answer to this point. A value of 0.193 was used for the anisotropy at zero time. The two-dimensional (τ, θ) plot is completely dominated by the cross-correlation peak associating the long lifetime with the long correlation time describing the Brownian motion of the protein (Figure 9B). A cross-correlation peak with a subnanosecond motion is also visible and a nanosecond flexibility as well, but they are very weak as compared to the main peak (~5−6% of the main peak in terms of $\Gamma_{(\tau, \theta)}$). From this analysis, the association of the shortest lifetime with rotational motion is not quite clear. The intermediate lifetime is not clearly defined either.

In an attempt to unmask the W89 emission, the protein was quenched by acrylamide as previously described. At 0.94 M acrylamide, the short lifetime was present in a much higher amount with respect to the long quenched one, as already described. The two-dimensional analysis of these data shows indeed that the short lifetime is here clearly associated with a (τ, θ) cross-correlation peak, with a correlation time of around 0.5 ns, close to that observed in FKBP12 (Figure 9C). The long lifetime is associated almost only with the rotational correlation time describing the Brownian motion of the protein and also with a nanosecond flexibility. This is a further argument for ascribing the short-lived emittor to the buried W89, which displays a similar nanosecond dynamics as in FKBP12.

Rotational Dynamics of the Trp Residues in FKBP59-I Complexes with FK506 and Rapamycin. According to the one-dimensional analysis of the rotational motions, the ligand binding to FKBP59-I suppresses the picosecond motion and the nanosecond flexibility in the complexes with both FK506 and rapamycin (Table 5). This kind of result could reflect the real physical changes associated with the complex formation with the immunosuppressant, *i.e.* a complete immobilization of the W59 indole ring. Owing to the lifetime heterogeneity persisting in both complexes, the

existence of specific (τ, θ) associations can, however, remain undetectable with the one-dimensional model.

The two-dimensional analysis was therefore performed for both complexes. The diagrams for both complexes are dominated by a major peak associating the Brownian rotation of the protein with the long lifetime (Figure 9D,E). In the case of the FKBP59-I/FK506 complex, the long lifetime population is also associated with a nanosecond flexibility, whereas it is not the case for the FKBP59-I/rapamycin complex. A minor peak reveals an association between the intermediate lifetime of 1 ns and either a subnanosecond rotation in the case of the FKBP59-I/FK506 complex or a nanosecond motion in the case of the FKBP59-I/rapamycin complex. The minor 0.2 ns lifetime class is not visible in this analysis. By comparison with the unliganded FKBP59-I, the main effect of FK506 binding on the protein local dynamics is therefore to suppress the subnanosecond rotational motion of the indole ring, to preserve and even enhance the amplitude, but to slow the rate of the segmental flexibility, which is likely that of the β-strand bearing the Trp59 residue. The rigidification effect induced by rapamycin binding appears stronger than for FK506. The suppression of the local flexibility induced by rapamycin may be due to the size of rapamycin, which is larger than FK506.

CONCLUSION

Domain I of FKBP59 (FKBP59-I), which is entirely responsible for the immunophilin character of the whole protein (PPIase activity and substrate specificity are similar to those of FKBP12), is shown by fluorescence spectroscopic techniques to display local changes in protein dynamics in a specific surface region, resulting from drug binding. The presence of two tryptophans located in two different environments (within the ligand binding site and on the external side of the β-sheet surface) enabled us to associate these major dynamics changes with the solvent-exposed face of a β-strand (50−61) and not with the hydrophobic cavity. Moreover, it appears that these dynamics changes elicited by both immunosupressants are not identical. These differential changes in dynamic properties of this particular region of the molecule upon ligand binding had not been observed in the immunophilin family of proteins, until recently, by proton exchange NMR experiments (Craescu *et al.*, 1996; Rouvière *et al.*, unpublished results). Whether these dynamic changes are also displayed in other surface regions of these proteins remains to be elucidated. Another question that is relevant to structure and/or dynamics−activity relationship concerns the differences by 1−2 orders of magnitude of both K_I or K_D values of the immunosuppressant drugs, observed with FKBP59-I as compared to FKBP12 (Renoir *et al.*, 1994; our present work). Up to now, these lower binding energies could not be readily explained by structural differences in the hydrophobic and aromatic residues of the active site since they are strictly conserved and positioned in the same manner as in FKBP12 (Craescu *et al.*, 1996). Moreover, the three-dimensional structure of the main chain remains unaltered upon ligand binding (Rouvière *et al.*, unpublished results). Whether this difference in binding energy could be explained by more subtle dynamic changes in other parts of the proteins remains to be explored.

It is therefore of particular interest to further study the influence of the immunosuppressive drug binding on the dynamics of FKBP59-I, particularly in its surface regions. In FKBP12, the absence of a highly sensitive fluorescent probe located on the outside of the binding site did not permit revelation of this kind of drug-induced conformational changes. To explore the effect of drug binding, a strategy involving Trp insertion in different locations along the protein sequence is under current development. The present study of the FKBP59 immunophilin domain may be extended to further investigate its interactions with immunosuppressant drugs and with new protein targets. Moreover, the aim is to explain the role of this particular domain in the integral, multifunctional protein, FKBP59, which also interacts with the heat shock protein of 90 kDa (hsp-90) and steroid receptors.

ACKNOWLEDGMENTS

We gratefully acknowledge the technical staff of LURE for running the synchrotron machine during the beam sessions. We thank Etienne-Emile Baulieu and Marie-Claire Lebeau (INSERM U33) for scientific support to this work and Marie-Claire Lebeau for comments on the manuscript. M.V. acknowledges the Institut National de la Santé et de la Recherche Médicale for continual financial support. We appreciate helpful discussions with Pr. A. P. Demchenko during the course of this work. Fujisawa and Wyeth-Ayerst are gratefully acknowledged for the gift of immunosuppressants.

REFERENCES

Alcala, J. R., Gratton, E., & Prendergast, F. G. (1987) *Biophys. J. 51*, 925−936.

Berlman, I. B. (1971) in *Handbook of Fluorescence Spectra of Aromatic Molecules*, Academic Press, New York.

Blandin, P., Mérola, F., Brochon, J.-C., Trémeau, O., & Menez, A. (1994) *Biochemistry 33*, 2610−2619.

Bouhss, A., Vincent, M., Munier, H., Gilles, A.-M., Takahashi, M., Bârzu, O., Danchin, A., & Gallay, J. (1996) *Eur. J. Biochem. 237*, 619−628.

Brochon, J.-C. (1994) *Methods Enzymol. 240*, 262−311.

Bushueva, T. L., Busel, E. P., Bushueva, V. N., & Burstein, E. A. (1974) *Stud. Biophys. 44*, 129−139.

Bushueva, T. L., Busel, E. P., & Burstein, E. A. (1975) *Stud. Biophys. 52*, 41−52.

Chambraud, B., Rouvière-Fourmy, N., Radanyi, C., Hsiao, K., Peattie, D. A., Livingston, D. J., & Baulieu, E.-E. (1993) *Biochem. Biophys. Res. Commun. 196*, 160−166.

Chen, R. F., Knutson, J. R., Ziffer, H., & Porter, D. (1991) *Biochemistry 30*, 5187−5195.

Cowgill, R. W. (1962) *Biochim. Biophys. Acta 133*, 6−18.

Cowgill, R. W. (1967) *Biochim. Biophys. Acta 140*, 37−44.

Craescu, C. T., Rouvière, N., Popescu, A., Cerpolini, E., Lebeau, M.-C., Baulieu, E.-E., & Mispelter, J. (1996) *Biochemistry 35*, 11045−11052.

De Lauder, W. B., & Wahl, Ph. (1971) *Biochim. Biophys. Acta 243*, 153−163.

Donzel, B., Gauduchon, P., & Wahl, Ph. (1974) *J. Am. Chem. Soc. 96*, 5001−5007.

Eftink, M. (1991) in *Topics in Fluorescence Spectroscopy, Vol. 2, Principles* (Lakowicz, J. R., Ed.) Chapter 2, pp 53−126, Plenum Press, New York.

Eftink, M. R., & Ghiron, C. A. (1976) *J. Phys.Chem. 80*, 486−493.

Eftink, M. R., & Ghiron, C. A. (1984) *Biochemistry 23*, 3891−3899.

Eftink, M., Wasylewski, Z., & Ghiron, C. A. (1987) *Biochemistry 26*, 8338−8346.

Flanagan, W., Corthesy, B., Bram, R., & Crabtree, G. (1991) *Nature 352*, 803−807.

Gallay, J., Vincent, M., Li de la Sierra, I. M., Alvarez, J., Ubieta, R., Madrazo, J., & Padrón, G. (1993) *Eur. J. Biochem. 211*, 213−219.
Gally, J. A., & Edelman, G. M. (1962) *Biochim. Biophys. Acta 60*, 499−509.
Gentin, M., Vincent, M., Brochon, J. C., Livesey, A. K., Cittanova, N., & Gallay, J. (1990) *Biochemistry 29*, 10405−10412.
Harrison, R. K., & Stein, R. L. (1990) *Biochemistry 29*, 1684−1689.
Ichiye, T., & Karplus, M. (1983) *Biochemistry 22*, 2884−2893.
Jaynes, E. T. (1983) *Papers on Probability Statistics and Statistical Physics* (Rosenkrantz, R. D., Ed.) Reidel, Dordrecht, The Netherlands.
Johnson, D. A., & Yguerabide, J. (1985) *Biophys. J. 48*, 949−955.
Kabsch, W., & Sander, C. (1983) *Biopolymers 22*, 2577−2637.
Kinosita, K., Jr., Kawato, S., & Ikegami, A. (1977) *Biophys. J. 20*, 289−305.
Kirby, E. P., & Steiner, R. F. (1970) *J. Phys.Chem. 74*, 4480−4490.
Klein, R., & Tatisheff, I. (1977) *Chem. Phys. Lett. 51*, 333−338.
Kuipers, O. P., Vincent, M., Brochon, J.-C., Verheij, H. M., de Haas, G. H., & Gallay, J. (1991) *Biochemistry 30*, 8771−8785.
Lakowicz, J. R., Joshi, N. B., Johnson, M. L., Szmacinski, H., & Gryczynski, I. (1987) *J. Biol. Chem. 262*, 10907−10910.
Lebeau, M.-C., Myagkikh, I., Rouvière-Fourmy, N., Baulieu, E.-E., & Klee, C. B. (1994) *Biochem. Biophys. Res. Commun. 203*, 750−755.
Le Bihan, S., Renoir, J.-M., Radanyi, C., Chambraud, B., Joulin, V., Catelli, M. G., & Baulieu, E.-E. (1993) *Biochem. Biophys. Res. Commun. 195*, 600−607.
Levitt, M., & Perutz, M. F. (1988) *J. Mol. Biol. 201*, 751−754.
Levy, R. M., & Szabo, A. (1982) *J. Am. Chem. Soc. 104*, 2073−2075.
Liang, J., Ealick, S., Nielsen, C., Schreiber, S. L., & Clardy, J. (1996a) *Acta Crystallogr. D52*, 207−210.
Liang, J., Hung, D. T., Schreiber, S. L., & Clardy, J. (1996b) *J. Am. Chem. Soc. 118*, 1231−1232.
Lipari, G., & Szabo, A. (1980) *Biophys. J. 30*, 489−506.
Liu, J., Farmer, J., Lane, W., Friedman, J., Weissman, I., & Schreiber, S. L. (1991) *Cell 66*, 807−815.
Livesey, A. K., & Brochon, J.-C. (1987) *Biophys. J. 52*, 693−706.
Livesey, A. K., & Skilling, J. (1985) *Acta Crystallogr., Sect. A: Fundam. Crystallogr. A41*, 113−122.
Livesey, A. K., Licinio, P., & Delahaye, M. (1986) *J. Chem. Phys. 84*, 5102−5107.
Lu, K. P., Hanes, S. D., & Hunter, T. (1996) *Nature 380*, 544−547.
Ludescher, R. D., Volwerk, J. J., de Haas, G. H., & Hudson, B. (1985) *Biochemistry 24*, 7240−7249.
Massol, N., Lebeau, M.-C., Renoir, J.-M., Faber, L. E., & Baulieu, E.-E. (1992) *Biochem. Biophys. Res. Commun. 187*, 1330−1335.
McMahon, L. P., Colucci, W. J., McLaughlin, M. L., & Barkley, M. D. (1992) *J. Am. Chem. Soc. 114*, 8442−8448.
Mérola, F., Rigler, R., Holmgren, A., & Brochon, J.-C. (1989) *Biochemistry 28*, 3393−3398.
Michnick, S. W., Rosen, M. K., Wandless, T. J., Karplus, M., & Schreiber, S. L. (1991) *Science 252*, 836−839.
Moore, J. M., Peattie, D. A., Fitzgibbon, M. F., & Thomson, J. A. (1991) *Science 252*, 836−839.
Park, S. T., Aldape, R. A., Futer, O., DeCenzo, M. T., & Livingston, D. J. (1992) *J. Biol. Chem. 267*, 3316−3324.
Perrot-Applanat, M., Cibert, C., Geraud, G., Renoir, J. M., & Baulieu, E.-E. (1995) *J. Cell Sci. 108*, 2037−2051.
Petrich, J. W., Chang, M. C., McDonald, D. M., & Fleming, G. R. (1983) *J. Am. Chem. Soc. 105*, 3824−3832.
Philips, L. A., Webb, S. P., Martinez, S. J., III, Fleming, G. R., & Levy, D. H. (1988) *J. Am. Chem. Soc. 110*, 1352−1355.
Radanyi, C., Chambraud, B., & Baulieu, E.-E. (1994) *Proc. Natl. Acad. Sci. U.S.A. 91*, 11197−11201.
Ricci, R. W., & Nesta, J. M. (1976) *J. Phys. Chem. 80*, 974−980.
Renoir, J. M., Le Bihan, S., Mercier-Bodard, C., Gold, A., Arjomandi, M., Radanyi, C., & Baulieu, E.-E. (1994) *J. Steroid Biochem. Mol. Biol. 48*, 101−110.
Ross, J. B. A., Wyssbrod, H. R., Porter, R. A., Schwartz, G. P., Michaels, C. A., & Laws, W. R. (1992) *Biochemistry 31*, 1585−1594.
Rotonda, J., Burbaum, J. J., Chan, H. K., Marcy, A. I., & Becker, J. W. (1993) *J. Biol. Chem. 268*, 7607−7609.
Rouvière-Fourmy, N., Craescu, C. T., Mispelter, J., Lebeau, M.-C., & Baulieu, E.-E. (1995) *Eur. J. Biochem. 231*, 761−772.
Shinitzky, M., & Goldman, R. (1967) *Eur. J. Biochem. 3*, 139−144.
Shizuka, H., Scrizawa, M., Shimo, T., Saito, I., & Matsuura, T. (1988) *J. Am. Chem. Soc. 110*, 1930−1934.
Silva, N. D., & Prendergast, F. G. (1996) *Biophys. J. 70*, 1122−1137.
Spencer, R. D., & Weber, G. (1970) *J. Chem. Phys. 52*, 1654−1663.
Steiner, R. F., & Kirby, E. P. (1969) *J. Phys. Chem. 73*, 4130−4135.
Stryjewski, W., & Wasylewski, Z. (1986) *Eur. J. Biochem. 158*, 547−553.
Suwaiyan, A., & Klein, U. K. A. (1989) *Chem. Phys. Lett. 159*, 244−250.
Szabo, A. G., & Rayner, D. M. (1980) *J. Am. Chem. Soc. 102*, 554−563.
Tai, P.-K. K., Maeda, Y., Nakao, K., Wakim, N. G., Duhring, J. L., & Faber, L. E. (1986) *Biochemistry 25*, 5269−5275.
Tai, P-K. K., Albers, M. W., Chang, H., Faber, L. E., & Schreiber, S. L. (1992) *Science 256*, 1315−1318.
Tilstra, L., Sattler, M. C., Cherry, W. R., & Barkley, M. D. (1990) *J. Am. Chem. Soc. 112*, 554−563.
Valeur, B., & Weber, G. (1977) *Photochem. Photobiol. 25*, 441−444.
Van Duuren, B. L. (1961) *J. Org. Chem. 26*, 2954−2960.
Van Duyne, G. D., Standaert, R. F., Karplus, P. A., Schreiber, S. L., & Clardy, J. (1991a) *Science 252*, 839−842.
Van Duyne, G. D., Standaert, R. F., Schreiber, S. L., & Clardy, J. (1991b) *J. Am. Chem. Soc. 113*, 7433−7434.
Van Duyne, G. D., Standaert, R. F., Karplus, P. A., Schreiber, S. L., & Clardy, J. (1993) *J. Mol. Biol. 229*, 105−124.
Vincent, M., & Gallay, J. (1991) *Eur. J. Biophys. 20*, 183−191.
Vincent, M., Brochon, J.-C., Mérola, F., Jordi, W., & Gallay, J. (1988) *Biochemistry 27*, 8752−8761.
Vincent, M., Li de la Sierra, I. M., Berberan-Santos, M. N., Diaz, A., Diaz, M., Padron, G., & Gallay, J. (1992) *Eur. J. Biochem. 210*, 953−961.
Vincent, M., Gallay, J., & Demchenko, A. P. (1995) *J. Phys. Chem.. 99*, 14931−14941.
Vos, R., & Engelborghs, Y. (1994) *Photochem. Photobiol. 60*, 24−32.
Wahl, Ph. (1979) *Biophys. Chem. 10*, 91−104.
Walker, M. S., Bednar, T. W., & Lumry, R. (1969) *Molecular Luminescence* (Lim, E. C., Ed.) W. A. Benjamin, New York.
Willis, K. J., Neugebauer, W., Sikorska, M., & Szabo, A. G. (1994) *Biophys. J. 66*, 1623−1630.

BI962289W